Journal of
Ceramic Science
and Technology

J. Ceram. Sci. Technol., **08** [3] 389-398 (2017)
DOI: 10.4416/JCST2017-00045
available online at: http://www.ceramic-science.com

Influence of Elevated Temperatures on the Mechanical Behavior of Jute-Textile-Reinforced Geopolymers

A.C. Constâncio Trindade[1], H.A. Alcamand[2], P.H. Ribeiro Borges[2], F. de Andrade Silva[*1]

[1]Department of Civil and Environmental Engineering,
Pontifical Catholic University of Rio de Janeiro (PUC-Rio), Brazil.
[2]Department of Civil Engineering, Federal Center for Technological
Education of Minas Gerais (CEFET-MG), Brazil.

received June 30, 2017; received in revised form July 28, 2017; accepted August 21, 2017

Abstract

Geopolymers may present important structural and environmental advantages compared to Portland-cement-based materials. They can achieve high mechanical strength at early ages and exhibit much better thermal durability than Portland-cement-based materials. Geopolymers are brittle materials and an increasing number of studies have been conducted on the incorporation of fibrous reinforcement into these matrices in recent years. Natural fibers appear as a reinforcing group that imply environmental superiority, resulting in improved mechanical behavior. This study evaluates the mechanical behavior of metakaolin-based geopolymers reinforced with jute textile when these are exposed to elevated temperatures. The matrices were activated with a combination of sodium-hydroxide and sodium-silicate solutions. Distinctions in the mixtures were made with the incorporation of different aggregates, i.e. natural quartz sand and chamotte. Direct tensile and compression tests were performed to study the mechanical behavior of the geopolymers when these were exposed to elevated temperatures. In addition, direct tensile tests were conducted on the fibers in different temperature conditions. X-ray diffraction and scanning electron microscopy (SEM) were used to investigate the microstructural changes of the reinforcement. The results indicated superior behavior for the matrices and composites made with the refractory aggregate, indicating a fiber-matrix interaction suitable for this combination at elevated temperatures.

Keywords: Geopolymers, composites, natural fibers, temperature

I. Introduction

The constant use of cementitious materials in large-scale projects around the world has driven the demand for alternative materials. The production of Portland cement (PC) is responsible for approximately 5 % of the global CO_2 emissions [1]. Its replacement by innovative materials such as "geopolymers" [2] presents a promising technological path for the construction industry. Geopolymers may be presented as an environmentally favorable option, since the production of its basic materials may reduce carbon emissions by up to six times [3].

Geopolymers are produced by means of alkali-activation of aluminosilicate materials; the activators are usually alkaline hydroxides and/or silicate solutions based on sodium and/or potassium [2,3]. The process of activation consists of the dissolution of the primary aluminosilicate structure, followed by the condensation of free silicates and aluminates, forming a 3D arrangement [2,3,4]. This configuration comprises cross-linked SiO_4 and AlO^-_4 tetrahedra, where the negative charge is balanced by the positive charges of the alkali ions (Na^+, K^+) [3,5,6]. Their microstructure, chemical and mechanical properties may vary significantly depending on the different sources of aluminosilicates; metakaolin (MK) and pulverized fly ash (PFA) are the most commonly used precursors [3,4]. The most prominent geopolymer applications are related to paving, precast concrete and repair technology [3,5,7].

Geopolymers are known to demonstrate good strength in elevated temperature conditions owing to their ceramic structure [8,9]. Kong *et al.* [9] showed that at extremely high temperatures (above 700 °C), MK-based geopolymers exhibit more severe degradation compared to PFA-based ones. However, at lower temperatures (< 500 °C) they exhibit similar mechanical properties and provide adequate stability without showing signs of spalling [8,9]. The authors also concluded that the incorporation of aggregates resulted in good mechanical performance at both room and elevated temperatures. It is important to note, however, that the use of incompatible aggregates results in unfavorable properties; the selection of an appropriate aggregate is paramount for each established condition [8,10,11].

Despite their superior mechanical response compared to PC-based materials [12], geopolymers are also fragile ceramics, characterized by low tensile strength and low strain ca-

* Corresponding author: fsilva@puc-rio.br

pacity. The incorporation of suitable proportions of man-made or natural fibers into the ceramic matrix is a practical solution to overcome the brittleness [13,14,15]. Recent studies [13,14,15,16] presented evidence of great improvements in the mechanical behavior of fiber-reinforced geopolymers, i.e. similar, or even superior performance when compared to PC-based cementitious composites. The incorporation of natural fibers in geopolymers is even more interesting in terms of environmental advantages [2,5,6].

The use of natural fibers consumes less energy and they do not pollute the environment since they are biodegradable materials. Natural fibers can be extracted from different plant parts, such as the stem (jute), leaf (sisal), and fruits (coir) [17,18]. Sankar and Kriven [14,15] investigated the microstructure and mechanical properties of geopolymeric composites reinforced with jute and fique fibers. In both studies [14,15], tensile and flexural tests were performed on as-received and alkali-treated fiber-reinforced composites. The results indicated higher tensile and flexural strength values for alkali-treated fiber-reinforced composites, owing to the removal of hemicellulose on alkali treatment, which promotes an increase in the elongation at breakage.

This work presents the results of an experimental investigation on the mechanical response of natural-fiber (jute)-reinforced MK-based geopolymers using different aggregates, under ambient conditions and after exposure to elevated temperatures. Compression and tensile tests were used to evaluate their mechanical response and crack formation. X-ray diffraction and scanning electron microscopy (SEM) were used to perform microstructural characterization of the reinforcement in such conditions.

II. Experimental

(1) Materials and processing

Metakaolin (MK) supplied by Metacaulim do Brasil was used as the aluminosilicate precursor. The activator solution was composed of a mixture of sodium hydroxide (NaOH) and sodium silicate solutions, so that the overall SiO_2/Na_2O molar ratio was equal to 1.21. Table 1 presents MK and sodium silicate chemical and physical properties, obtained by means of X-ray fluorescence (XRF) and from supplier's reports, respectively.

Natural quartz sand and chamotte 70 (CHA) were used as aggregates. Quartz sand exhibited a density of 2.68 g/cm³, fineness modulus of 2.28, and maximum diameter of 1.18 mm. The refractory aggregate exhibited a density of 2.66 g/cm³, apparent porosity equal to 6.3 %, and maximum diameter of 1.18 mm. Quartz sand and chamotte were sieved to determine the particle size distribution (PSD); the PSD of MK was obtained with laser diffraction granulometry. D95 corresponds to the diameter below which 95 % of the mass is found; the D95 results obtained for each material were: 15 μm, 875 μm, and 1040 μm, respectively for MK, chamotte and sand.

Table 1: Chemical and physical properties of metakaolin and sodium silicate solution.

Chemical Compositions	Metakaolin (MK)	Sodium Silicate Solution
SiO_2	55.50 %	32.20 %
Al_2O_3	36.50 %	-
Fe_2O_3	2.00 %	-
TiO_2	1.00 %	-
K_2O	1.70 %	-
Na_2O	0.10 %	14.70 %
H_2O	-	53.10 %
LoI	3.20 %	
Density (g/cm³)	2.58	1.57

A natural jute plain weave obtained from the state of Pará (Brazil) was used as reinforcement in the geopolymer composites. This natural fiber is obtained from the stem of the plant *Corchorus capsularis*, and it is extracted in a combination of processes: (i) cutting, (ii) retting, (iii) shredding, (iv) drying, (v) packing, and (vi) classification [19]. The jute fabric is formed by yarns aligned in both directions, each yarn containing at least a hundred filaments [19].

The jute fiber presents high amounts of cellulose and hemicellulose [20]; its chemical composition was determined according to the procedures suggested by Wallis *et al.* [21], which gives the absolute content values. The analyses were performed using DIONEX equipment with HPAEC high-performance liquid chromatography, equipped with detectors by pulsed amperometry. This method aimed to evaluate the fine chemistry of samples of lignocellulosic materials regarding their carbohydrate (cellulose and hemicellulose) and acid lignin contents. The results are presented in Table 2. The components are expressed in percentage based on the dry weight of the extractive material. The cellulose content (74.4 %) is mainly responsible for the mechanical strength of the fiber [19], while lignin content (8.43 %) is directly related to the bonding of filaments that form a yarn.

Table 2: Quantitative chemical composition of the lignocellulosic material - jute.

Fiber	Insoluble lignin	Soluble lignin	Total lignin	Cellulose	Hemicellulose	Remaining content
Jute	6.62 %	1.81 %	8.43 %	74.4 %	15.0 %	2.17 %

Three geopolymer formulations were studied (Table 3), all of which obtained by means of the activation of MK; the composition of the matrix (molar ratios) was based on the studies of Borges *et al.* [22]. The distinction between the three formulations was the presence and type of aggregate: (i) plain matrix (no aggregate); (ii) natural sand; (iii) chamotte 70. From all characteristics pre-

viously mentioned, the mixtures were named: 100MK, 100MK+SAND, and 100MK+CHA.

The mixes were batched in a 5-L-capacity planetary mixer as follows: (i) manual pre-mixing of the dry materials (sand/chamotte, MK); (ii) addition of the alkaline activator solutions (premixed); (iii) mixing for 4 min at 136 rpm; (iv) pause in the mixing procedure to scrape the bowl to get unmixed materials adhering to the wall; (v) final mixing and homogenization for 3 min at 281 rpm.

Table 3: Solid materials and molar ratios of the geopolymer matrix (100MK), and also of the aggregate-reinforced geopolymers (100MK+SAND and 100MK+CHA).

Formulation	*MK/ Sand*	*MK/ CHA*	SiO_2/Al_2O_3	H_2O/Na_2O	Na_2O/SiO_2	Na_2O/Al_2O_3
100MK +SAND	1.00	-	3.00	11.00	0.25	0.75
100MK +CHA	-	0.50	3.00	11.00	0.25	0.75
100MK	-	-	3.00	11.00	0.25	0.75

The consistency of the mixes (100MK+SAND, 100MK +CHA, and 100MK) was determined using the flow table test, following the procedures described by the ASTM C1439 [23] (Fig. 1a). The results obtained were: (i) 127.5 mm for 100MK+SAND; (ii) 175.5 mm for 100MK+CHA; and (iii) 212.0 mm for 100MK. It is possible to observe that the workability increased as the proportion of aggregates incorporated into the matrix decreased, and the highest consistency was reached for the plain matrix (100MK).

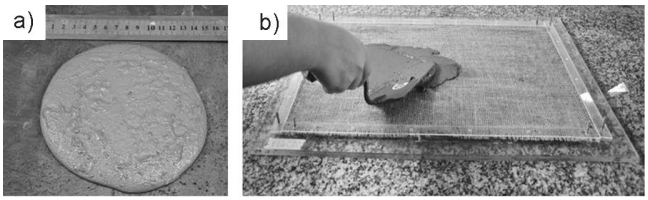

Fig. 1: (a) Flow table test performed with a geopolymer matrix, and (b) molding system of composites reinforced with textile jute fiber.

Cylindrical specimens (50 x 100 mm, diameter x height) were cast for compression tests. Plate specimens (450 x 60 x 12 mm; length x width x thickness) reinforced with bi-directional arrangements of jute fabrics were cast in an acrylic mold (Fig. 1b) for tensile tests. The jute fabric was engineered in a plain weave configuration where each weft yarn crosses the warp by going over one and then under the next yarn. The fabric presented a constant mesh opening equal to 3.7 x 2.85 mm. The jute yarn presented a linear density equal to 326 tex (mass in g of 1000 m of yarn). To manufacture the composites, five layers of fibers were used, with a total volumetric fraction of 10 % alternating with layers of geopolymers (2 mm each) up to a thickness of 12 mm. The fibrous reinforcement was stretched and secured to the cast screws. The consistency of the geopolymers was such that they did not require any type of consolidation.

All specimens were prepared and cured at room temperature (25 ± 2 °C), demolded after 24 h and wrapped in plastic bags to prevent moisture loss and cracking during the subsequent curing over seven days. The curing regime was established according to the results found by Borges *et al.* [22].

(2) Testing methods

The compressive strength was tested for unreinforced geopolymers, using a MTS-810 servo-hydraulic machine, with a load capacity of 500 kN. The tests complied with ASTM C39 [24], with a displacement rate of 0.5 mm/min. The elastic modulus was computed in the linear elastic region up to 40 % of the maximum strength.

Direct tensile tests were performed for jute-reinforced composites; a MTS universal servo-controlled testing system, model 311, was used. The tests were conducted using a displacement rate of 1.0 mm/min. The displacements were measured by two LVDTs positioned on the sides of the specimens with 250-mm gauge length, and only the average value obtained through the readings was considered. Fig. 2 presents the tensile test arrangement. The specimens were fixed in steel plates with screws (torque = 10 N·m). For the mechanical analysis, three specimens of each formulation, cured at room temperature, were subjected to testing at seven days of age.

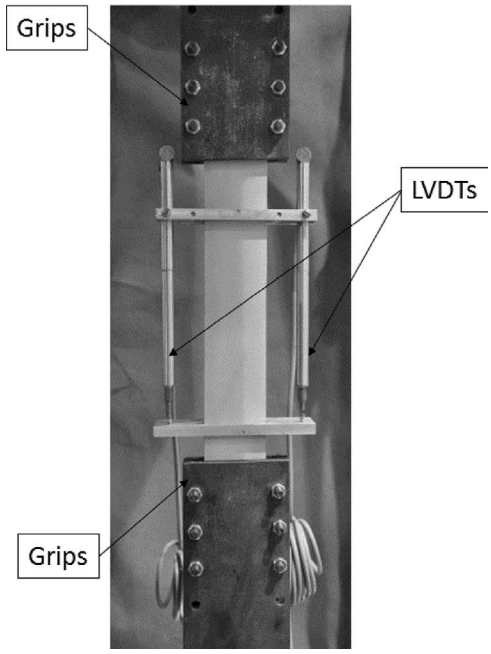

Fig. 2: Direct tensile test arrangement for the composites.

Compressive strength testing was performed at room temperature as well as at high temperature (100 °C, 300 °C and 500 °C). The cylinders were exposed to different temperatures in a muffle furnace, at a heating rate of 10 K/min. The samples were kept for 1 h at the desired temperature, after which they were allowed to cool down naturally inside the furnace.

For the tensile tests, however, the composites were exposed to lower temperatures, since the natural fibers reach their highest degradation at approximately 230 °C. Therefore, the specimens (in groups of three) were exposed to temperatures of 100, 150, 200, and 250 °C, achieved at the same heating rate (10 K/min).

Direct tensile tests of the fibers were performed in a servo hydraulic mechanical testing system model MTS-810, with a load cell of 100 N to correctly measure the applied load. The tests were performed at a displacement rate of 0.1 mm/min; an LVDT coupled to the grips was used to correctly measure the displacement. The samples were glued to a paper template (140 g/m^2), in accordance with ASTM C1557 [25], for a better alignment inside the grips. Fig. 3 shows the test arrangement and the detail of the specimen. The tests were performed for fiber lengths of 20 mm, initially at room temperature. Subsequently, fiber specimens were also tested in tension after being subjected to the same elevated temperatures as the composites (100 °C, 150 °C, 200 °C and 250 °C). Finally, jute fibers were extracted from untested 100MK+CHA composites exposed to 250 °C, and were also evaluated in tension in order to assess the performance of the fibers at high temperature when protected inside the matrix during exposure. Fifteen fiber specimens were tested for each condition.

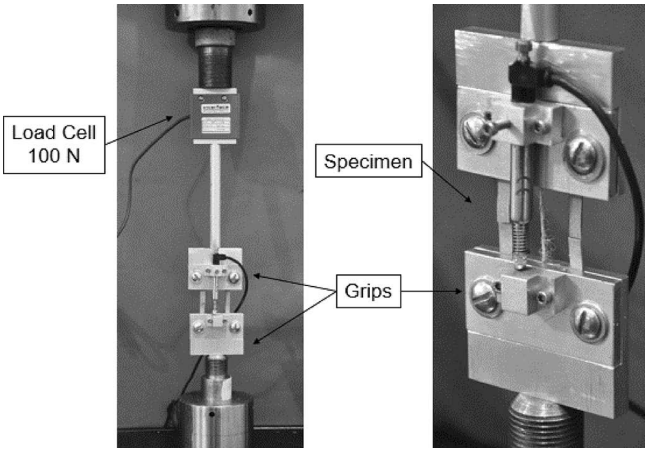

Fig. 3: Direct tensile test arrangement for the fibers.

XRD was used to assess the degradation of fibers under high temperature. The fibers exposed to 25 °C, 100 °C, 150 °C and 200 °C were milled in a knife mill to reduce the particle size. XRD was performed on a Shimadzu XRD-7000 with copper radiation (Cu-kα, λ = 1.5418 Å), operating at 40 kV and 30 mA, scanning at 1° per minute and step size of 0.02° between 10 and 40° (Bragg angles - 2θ). The crystallinity index of the fibers was calculated with the intensity results obtained for the crystalline and amorphous fractions, according to the method proposed by Müller *et al.* [26]:

$$\mathrm{CrI}\,(\%) = \frac{A_{cr}}{A_t} \times 100 \qquad (1)$$

where A_{cr} corresponds to the crystalline correspondent area, and A_t to the total area, comprising both crystalline peaks and amorphous hump. The values of A_{cr} and A_t were computed using the software Grapher version 8, using the command "Calculate Area". This tool allowed the interest intervals to be selected and their respective areas obtained in the diffractograms (crystalline and amorphous sums).

The fibers' morphology was investigated using an SEM JEOL JSM-6510 LV. The microscope was operated under an accelerating voltage of 20 kV. Samples as received and withdrawn from the composites exposed to elevated temperatures were examined.

III. Results and Discussion

Fig. 4.a and Table 4 show the effect of the temperature on the compressive strength of the three formulations. Fig. 4.b shows the normalized strength losses (NS_{Loss}) in the same temperature range. For each formulation, the normalized strength loss was calculated as per Equation 2, so that 0 on the y-axis equals the strength in ambient conditions:

$$\mathrm{NS_{Loss}}\,(\%) = 1 - \frac{\mathrm{CS_{Ti}}}{\mathrm{CS_{T.amb}}} \times 100 \qquad (2)$$

where:

$\mathrm{CS_{Ti}}$ = compressive strength at a given temperature;

$\mathrm{CS_{T.amb}}$ = compressive strength at room temperature.

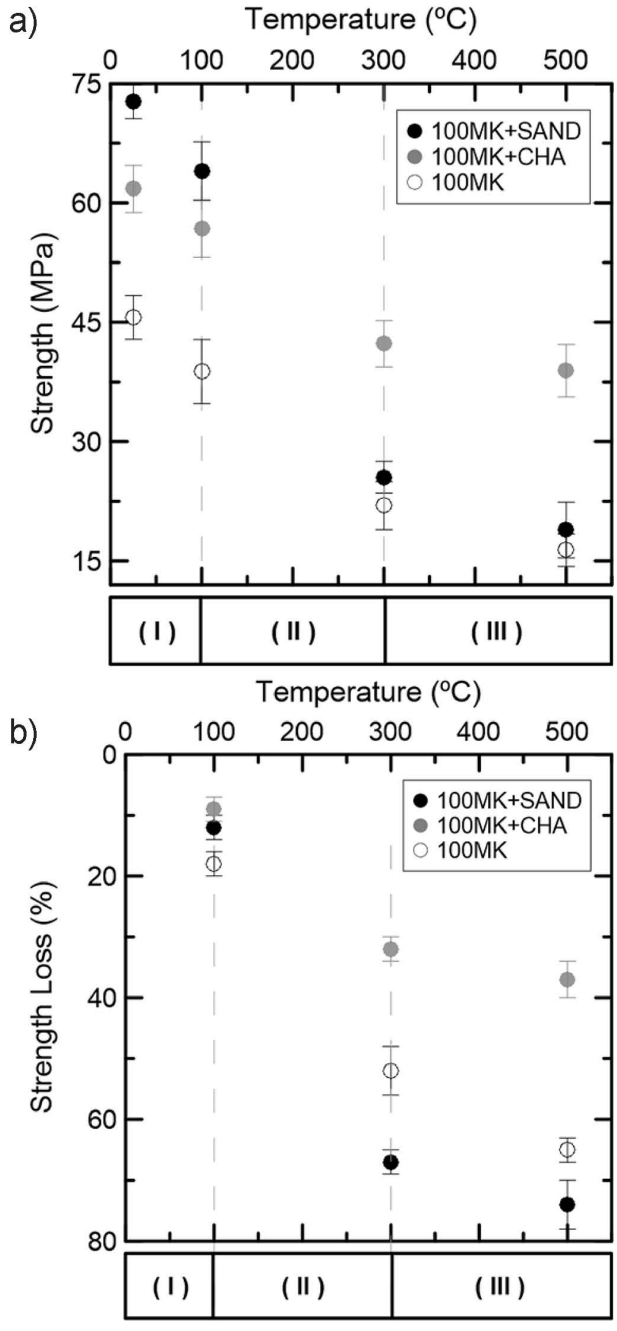

Fig. 4: Effect of temperature on the compressive strength of different geopolymer formulations: (a) absolute and (b) percentage strength loss.

Table 4: Compressive strength and Young's modulus of different geopolymer formulations after the exposure to different temperatures (standard deviation values in parentheses).

Formulation	Temperature							
	25 °C		100 °C		300 °C		500 °C	
	σ_{max} (MPa)	E_c (GPa)	σ_{max} (MPa)	E_c (GPa)	σ_{max} (MPa)	E_c (GPa)	σ_{max} (MPa)	E_c (GPa)
100MK+SAND	72.70 (±2.12)	14.26	64.03 (±3.65)	11.01	25.53 (±2.0)	2.91	18.88 (±3.5)	1.63
100MK+CHA	61.73 (±2.96)	14.70	56.7 (±3.54)	12.06	42.3 (±2.91)	5.78	38.86 (±3.3)	3.99
100MK	45.65 (±2.75)	10.61	38.81 (±4.01)	8.10	21.94 (±3.02)	2.35	16.35 (±2.04)	1.54

σ_{max} = maximum strength; E_c = Young'smodulus.

Overall, it is possible to notice the reduced compressive strength for the plain matrix (100 MK) at room temperature. In fact, the 100MK+SAND formulation presented the highest strength (72.7 MPa), followed by 100MK+CHA (61.73 MPa); meanwhile 100MK achieved 45.65 MPa. Geopolymers made from the activation of MK produce a characteristic gel Na_2O-Al_2O_3-SiO_2-(H_2O)(N-A-S-(H)) [22], resulting in a somewhat porous, micro-cracked and permeable matrix. The inclusion of compatible aggregates reduces the micro-cracks, increasing the stiffness and the strength of the material.

The results of the Young's modulus (E_c) tests (Table 4) at room temperature were quite similar for the three formulations, i.e. 14.7, 14.26 and 10.61 GPa for 100MK+CHA, 100MK+SAND and 100MK, respectively. In fact, geopolymers do not present a linear relationship between compressive strength and E_c; an intrinsic modulus of elasticity between 17 – 18 GPa was reported in the literature [27] for the N-A-S-(H) gel, irrespective of changes in the formulation.

Fig. 4a, and Table 4 also present the degradations of all geopolymer formulations when exposed to elevated temperatures. The degradation processes can be divided into three phases. Phase I corresponds to degradations occurring at temperatures up to 100 °C. In this range, it is possible to observe small reductions in strength (σ_{max}) and Young's modulus (E_c) for all geopolymers. These reductions are related to the loss of free water contained in the pores of the matrices [10, 28]. Phase II corresponds to degradations occurring between 100 and 300 °C. At this temperature range, when the dehydration of the structures present in the geopolymer gels occur [9, 28, 25], it is possible to observe similar degradations (in proportion) (Fig. 4b) for the formulations 100MK+CHA and 100MK. In contrast, 100MK+SAND presented the largest decrease in strength and modulus, owing to the incompatibility of the aggregate with the matrix in such temperature conditions.

At this point, the quartz aggregate begins to suffer irreversible damage, disrupting the matrix interface, until it reaches Phase III. In this region, corresponding to temperatures between 300 and 500 °C, the degradation of the quartz sand [28], along with the formation of microcracks in the matrix [28, 29], promotes intense losses in the mechanical behavior for 100MK+SAND. However, the behavior of the formulations 100MK+CHA and 100MK did not change significantly in this temperature range, with results still significantly high for 100MK+CHA (compressive strength of 38.86 MPa), a consequence of an important compatibility between materials.

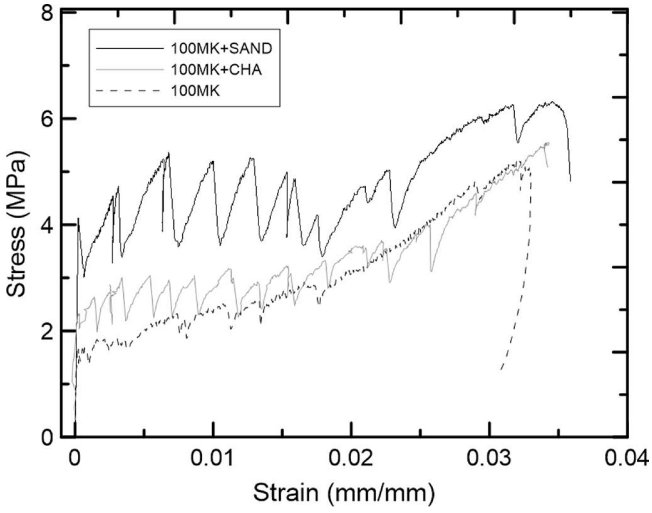

Fig. 5: Direct tensile test results of the natural-fiber-reinforced geopolymers: 100MK+SAND, 100MK+CHA, and 100MK.

The results of the direct tensile tests for the three composites reinforced with jute fabrics are presented in Figs. 5 and 6, for room temperature and after high-temperature exposure, respectively. Table 5 summarizes all data. Fig. 5 shows different responses at different stages of loading, from the macroscopic point of view. Analogous to the analysis made by Silva *et al.* [18] (for cementitious composites), it can be stated that in the initial region, i.e. the linear elastic phase, both matrix and fiber behave linearly. The stiffness of the composites is controlled by the properties of the matrix. This behavior is interrupted by the formation of the first crack. At this point, it can be observed that the composite 100MK+SAND presented a significant increase in the first cracking strength (σ_{1f}), reaching 4.13 MPa, compared to 2.31 and 1.37 MPa obtained for the 100MK+CHA and 100MK composites, respectively. These results are in line with the compressive strength previously discussed.

Table 5: Tensile stress and Young's modulus of different geopolymer composites after the exposure to different temperatures (standard deviation values in parentheses).

Composite	Temperature														
	25 °C			100 °C			150 °C			200 °C			250 °C		
	σ_{1f} (MPa)	σ_u (MPa)	E_t (MPa)	σ_{1f} (MPa)	σ_u (MPa)	E_t (MPa)	σ_{1f} (MPa)	σ_u (MPa)	E_t (MPa)	σ_{1f} (MPa)	σ_u (MPa)	E_t (MPa)	σ_{1f} (MPa)	σ_u (MPa)	E_t (MPa)
100MK +SAND	4.13 (±0.51)	6.31 (±0.78)	14.92 (±1.37)	1.43 (±0.42)	3.86 (±0.67)	9.35 (±0.96)	1.05 (±0.38)	2.26 (±0.78)	5.39 (±0.71)	–	–	–	–	–	–
100MK +CHA	2.31 (±0.29)	5.54 (±0.48)	14.04 (±1.06)	2.10 (±0.27)	3.67 (±0.62)	10.42 (±1.19)	1.87 (±0.34)	2.86 (±0.81)	10.03 (±1.11)	1.16 (±0.18)	2.39 (±0.63)	8.01 (±0.95)	0.41 (±0.09)	1.53 (±0.56)	4.22 (±0.43)
100MK	1.37 (±0.18)	5.21 (±0.76)	10.53 (±1.18)	1.24 (±0.12)	3.84 (±0.88)	8.67 (±1.02)	0.76 (±0.07)	3.15 (±1.01)	6.76 (±0.85)	0.60 (±0.09)	2.11 (±1.01)	5.30 (±1,33)	–	–	–

σ_{1f} = tensile stress in first crack; σ_u = ultimate tensile stress; E_t = Young'smodulus.

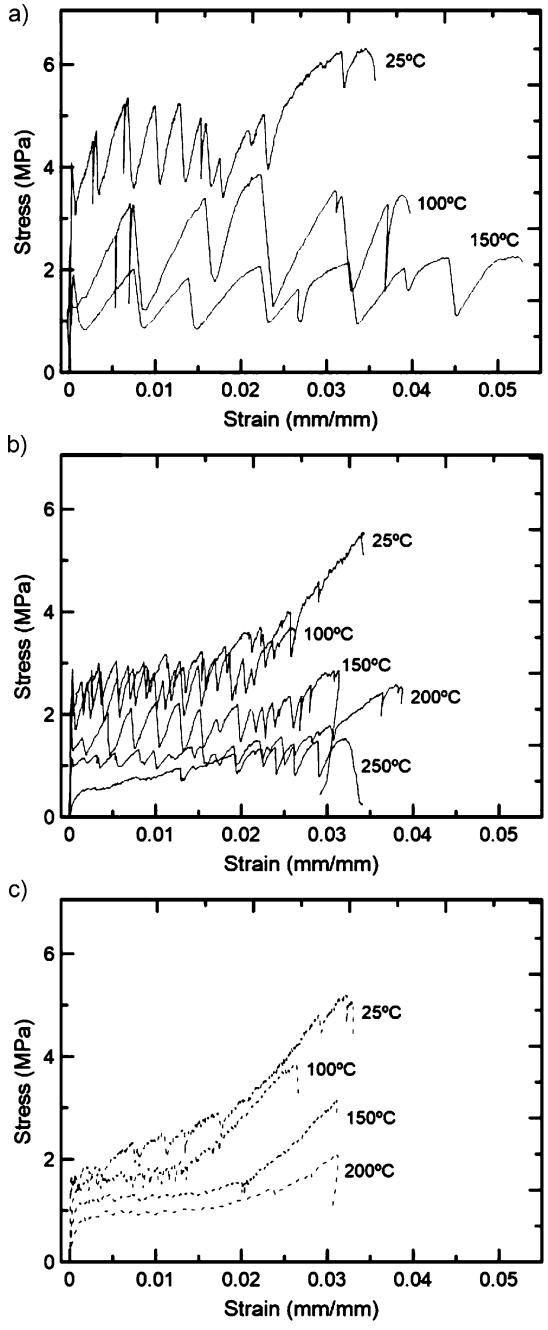

Fig. 6: Tensile test results of the jute-fiber-reinforced composites after exposure to different temperatures: (a) 100MK+SAND, (b) 100MK+CHA, and (c) 100MK.

After the formation and propagation of cracks in a distributed manner in the composite, it is possible to observe that the load-bearing capacity of the three composites was not exhausted. The composite 100MK+SAND, despite the highest mechanical tensile strength, presented higher cracking opening and a significantly lower number of cracks formed during the test. In contrast, composites 100MK+CHA and 100MK presented lower cracking opening and a significantly higher number of cracks. This mechanism may be associated with the improved workability of the mixes. A higher flow table spreading results in a better matrix penetration into the filaments and textile layers of the jute fibers, promoting an improved stress transfer mechanism. This superior behavior allows the formation and propagation of a larger number of cracks, increasing the ultimate strength (σ_u). All composites, even with different mechanical responses of their formulations, reached equivalent ultimate strength, strain-hardening and multiple cracking formation.

The results of the direct tensile tests for the composites exposed to elevated temperatures are presented in Fig. 6 (a, b, c) and in Table 5. The 100MK+SAND composite (Fig. 6a) presented the lowest mechanical capacity at elevated temperatures. This vulnerability is a direct result of the more severe degradations taking place in the material, effect of the weakness in the paste-aggregate interfacial transition zone (ITZ). This composite only presented the capacity to form multiple cracks and obtain strain-hardening behavior up to 150 °C, but above this temperature, it presented significant losses in mechanical strength and Young's modulus.

Unlike 100MK+SAND, composite 100MK+CHA presented a strain-hardening behavior and multi cracking up to 250 °C (Fig. 6b), in spite of reductions in the ultimate strength as the temperature increased. This composite presented a reduced number of cracks and still managed to withstand temperatures considered extreme for the jute fiber. This ability to maintain adequate behavior in elevated temperatures conditions can be related, once again, to a better compatibility in the paste-aggregate ITZ and its fluidity. The 100MK formulation presented the lowest mechanical strength of those studied; however, the results were remarkable when this geopolymer was reinforced with jute fibers and exposed to elevated temperatures. The

curves shown in Fig. 6c not only present losses in the mechanical capacity of the composite 100MK at each elevated temperature, but also an apparent improvement in the fiber-matrix interaction. This improvement is evidenced by the formation of a large number of cracks with smaller openings.

However, not only the geopolymer matrix plays a significant role in the fiber-matrix interaction. It is also important to analyze the reinforcement under extreme conditions to fully comprehend this behavior.

The results of the direct tensile tests for the jute yarns exposed to different temperatures are presented in Fig. 7 and Table 6. The results show a higher strength and strain capacity for the fiber at room temperature. Stiffness and strength reductions occur for the fibers exposed to 100 °C and 150 °C. However, an adverse behavior occurs when the fiber is exposed to 200 °C; its strain capacity undergoes a reduction, increasing its stiffness and Young's modulus. On the other hand, the fiber exposed to 250 °C presented significant strength losses. The fiber removed from the 100MK+CHA composite exposed to 250 °C, exhibited better mechanical behavior than the fiber simply exposed to this temperature. This may be due to the fact that the geopolymer matrix is working as a protective layer around the natural fiber, therefore mitigating its degradation process. The microstructural analysis performed in this study, presented hereafter, will help to evaluate any chemical and structural modifications under high temperatures.

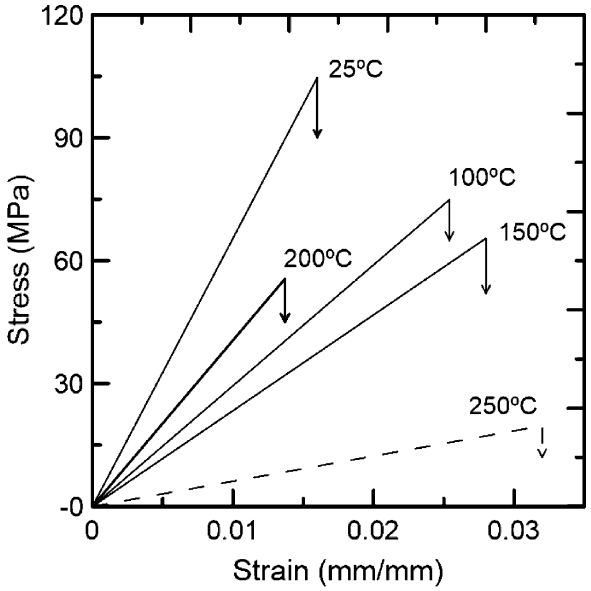

Fig. 7: Tensile behavior of jute fibers at room temperature, after being exposed to elevated temperatures (100, 150, and 200 °C), and after being removed from the 100MK+CHA composite exposed to 250 °C.

Fig. 8 presents the diffractograms for different exposure temperatures of the jute fiber. It is possible to observe that the crystalline peaks for cellulose (2θ = 15.32° and 2θ = 22.28°) are present in all temperature variations. The crystallinity indexes (relating maximum and minimum intensity peaks) obtained for each temperature are shown in Table 7. It is generally accepted that higher crystallinity indexes correspond to higher stiffness, and lower strain capacities [26, 31]. Taking this into consideration, it is possible to correlate the values obtained in Table 7 with the fiber tensile results (Fig. 9). It can be observed that the highest crystallinity index obtained occurred for the fiber maintained in room temperature. From this temperature, up to 150 °C, a gradual reduction takes place, indicating losses in fiber stiffness. However, a distinct behavior occurs for the fiber exposed to 200 °C, since the crystallinity index increases once more. This fact reinforces the results presented in the direct tensile tests of the fiber, where the jute exposed to 200 °C presented higher stiffness, despite showing loss in strength. These results also support the behavior obtained with the composites 100MK+CHA and 100MK when submitted to this temperature range.

Table 6: Results of tensile tests for jute fibers after exposure to different temperature conditions (standard deviation values in parentheses).

Temperature	Max Load (N)	Tensile strength (MPa)	Strain capactity (mm/mm)	Young's modulus (GPa)
25 °C	50.67 (±13.64)	104.75 (±26.8)	0.017 (±0.007)	6.16 (±0.75)
100 °C	36.23 (±11.85)	74.9 (±24.49)	0.025 (±0.006)	2.98 (±0.62)
150 °C	31.67 (±7.92)	65.47 (±14.56)	0.028 (±0.004)	2.33 (±0.58)
200 °C	26.88 (±8.26)	55.58 (±13.89)	0.013 (±0.005)	4.03 (±0.51)
250 °C	-	-	-	-
Removed 100MK+CHA 250 °C	9.5 (±3.83)	19.67 (±7.92)	0.032 (±0.007)	0.68 (±0.23)

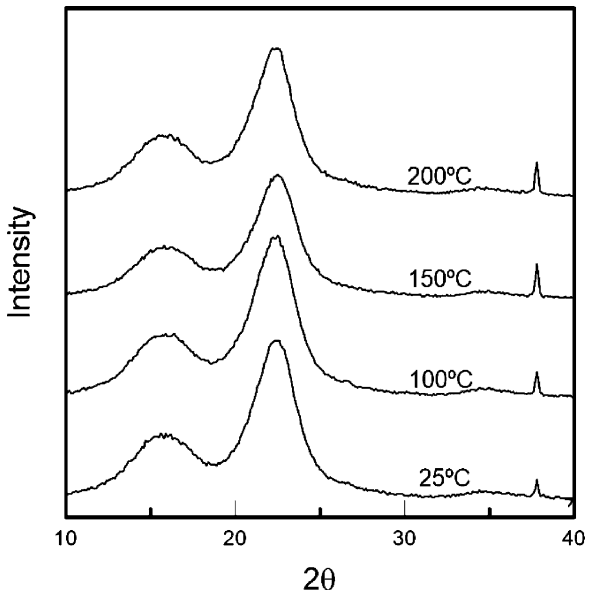

Fig. 8: X-ray diffractograms of the jute fibers: (a) at room temperature, and after being exposed to (b) 100 °C, (c) 150 °C and (d) 200 °C.

Table 7: Summary of crystallinity values (Crl) of jute fibers after exposure to different temperature conditions.

Temperature	Crystallinity (%)
25 °C	37.6
100 °C	32.2
150 °C	21.7
200 °C	27.8

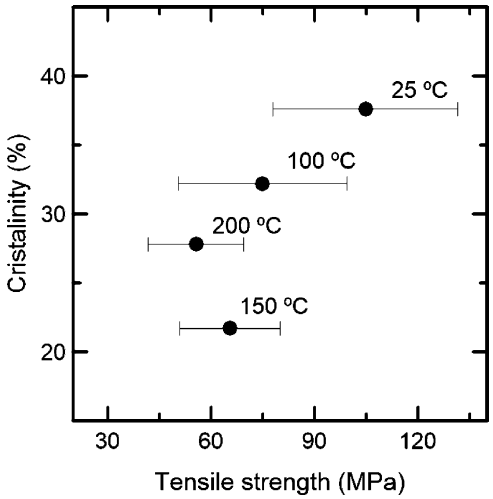

Fig. 9: Correlation between crystallinity and tensile strength at different temperatures.

Fig. 10 presents the micrographs of the fibers in two distinct conditions: (i) as-received and (ii) removed from untested 100MK+CHA composite exposed to 250 °C. The cross-sections and their longitudinal profiles were evaluated. Fig. 10a shows the characteristic cross-section of the natural fibers, formed by several fiber cells joined by the middle lamella (lignin) [19,31]. Each fiber cell is formed by four structures: primary, secondary, and tertiary walls, and lumens [18,19,31]. It is possible to observe the deterioration of the fiber in Fig. 10b, with consequent reduction of the cross-sectional area and the closing of the lumens occurring with the rise in temperature. These processes interfere in the stiffness and in strength of the fiber [19]. However, despite showing signs of degradation (mainly due to the disappearance of lumens), the fiber is still able to maintain its integrity at a temperature considered extreme for natural materials. Figs. 10c and 10d present the longitudinal profiles of the fibers in both conditions. The fiber as received presents a well-defined structure with aligned fiber cells. Again, the fiber removed from the composite exposed to 250 °C shows signs of degradation, but still presents a continuous structure. This occurs owing to the excellent behavior at elevated temperatures of the 100MK+CHA matrix, that appears to mitigate the fiber degradation, allowing an adequate strain capacity of the composite.

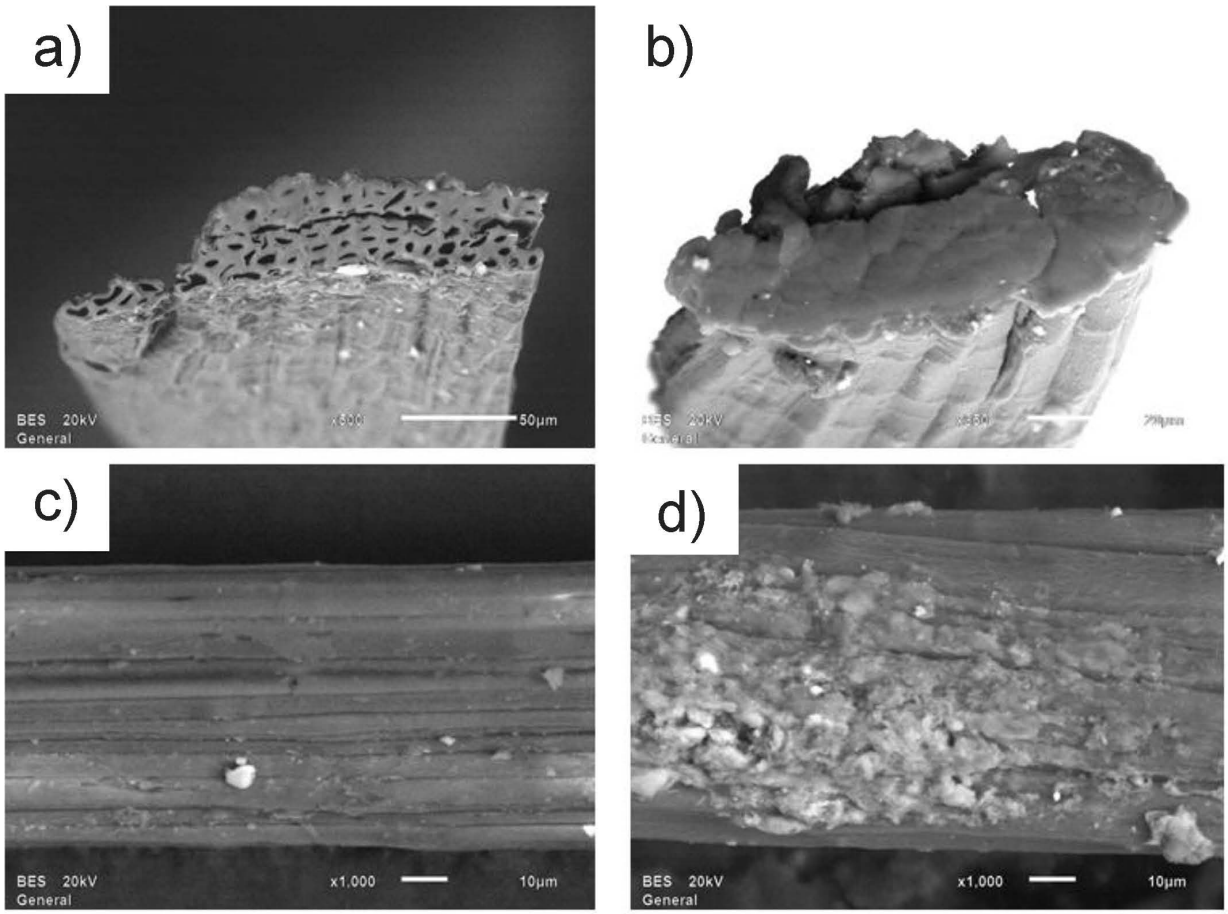

Fig. 10: Jute fibers' cross-section morphology and longitudinal profiles: (a) and (c) at room temperature as received; (b) and (d) after being removed from the 100MK+CHA composite exposed to 250 °C.

IV. Conclusions

Geopolymers based on metakaolin produce a characteristic gel (N-A-S-(H))that results in a porous, microcracked and permeable matrix (100MK). The incorporation of aggregates, such as quartz sand (100MK+SAND) and chamotte (100MK+CHA), significantly improves the mechanical response. Under high temperature conditions the incorporation of aggregates may result in different responses depending on their mineralogy and interfacial transition zone. The results of the present work showed that the incorporation of the refractory aggregate, chamotte (100MK+CHA), exhibited higher strength in all studied temperatures.

The three composites reinforced with natural fibers showed a strain hardening behavior with multiple crack formation under tensile loading. The fluidity of the matrices and their interfacial transition zones appears as main factors in the strain capacity of the composites. The composites 100MK+CHA and 100MK, although not reaching first crack strengths as high as the composite 100MK+SAND, demonstrated a superior strain hardening behavior with a higher cracking density and smaller crack widths.

It is possible to conclude that the incorporation of natural fibers in geopolymers appears a viable solution to overcome its initial brittle behavior. Under elevated temperatures, geopolymer composites produced with chamotte aggregates and without any aggregates can present favorable mechanisms to withstand the degradation of the natural jute fiber at elevated temperatures, presenting high strength and adequate strain capacity.

References

1 Huntzinger, D.N., Eatmon, T.D.: A life-cycle assessment of portland cement manufacturing: comparing the traditional process with alternative technologies, *J. Clean. Prod.*, **17**, [7], 668 – 675, (2009).

2 Davidovits, J.: Chemistry of geopolymeric systems, terminology, *Geopolymer*, **99**, 9 – 39, (1999).

3 Vickers, L., Van Riessen, A., Rickard, W.D.: Fire-resistant geopolymers: Role of fibres and fillers to enhance thermal properties. Springer, New York 2015.

4 Rovnaník, P.: Effect of curing temperature on the development of hard structure of metakaolin-based geopolymer, *Constr. Build. Mater.*, **24**, [7], 1176 – 1183, (2010).

5 Provis, J.L., Van Deventer, J.S.J.: Geopolymers: Structures, processing, properties and industrial applications. Elsevier, 2009.

6 Davidovits, J.: Properties of geopolymer cements. In: 1st International Conference on Alkaline Cements and Concretes (Vol. 1, pp. 131 – 149).

7 Davidovits, J.: Years of successes and failures in geopolymer applications. Market trends and potential breakthroughs. In: Keynote Conference on Geopolymer Conference, 2008.

8 Kong, D.L., Sanjayan, J.G.: Effect of elevated temperatures on geopolymer paste, mortar and concrete, *Cement Concrete Res.*, **40**, [2], 334 – 339, (2010).

9 Kong, D. L., Sanjayan, J. G., Sagoe-Crentsil, K.: Comparative performance of geopolymers made with metakaolin and fly ash after exposure to elevated temperatures, *Cement Concrete Res.*, **37**, [12], 1583 – 1589, (2007).

10 Barbosa, V.F.F., Mackenzie, K.J.D.: Thermal behaviour of inorganic geopolymers and composites derived from sodium polysialate, *Mater. Res. Bull.*, **38**, [2], 319 – 331, (2003).

11 Musil, S.S., Kriven, W.M.: *In Situ* mechanical properties of chamotte particulate reinforced potassium geopolymer, *J. Am. Ceram. Soc.*, **97**, [3], 907 – 915, (2014).

12 Pan, Z., Sanjayan, J.G., Rangan, B.V.: Fracture properties of geopolymer paste and concrete, *Mag. Concr. Res.*, **63**, [10], 763 – 771, (2011).

13 Nematollahi, B., Sanjayan, J., Ahmed Shaikh, F.U.: Tensile strain hardening behavior of PVA fiber-reinforced engineered geopolymer composite, *J. Mater. Civil Eng.*, **27**, [10], 04015001, (2014).

14 Sankar, K.; Kriven, W.M.: Sodium geopolymer reinforced with jute weave. *Ceram. Eng. Sci. Proc.*, **35**, [8], 39 – 60, (2014).

15 Sankar, K.; Kriven, W. M.: Potassium geopolymer reinforced alkali-treated fique, *Ceram. Eng. Sci. Proc.*, **35**, [8], 61 – 78, (2014).

16 Welter, M., Schmuecker, M., MacKenzie, K.J.D.: Evolution of the fibre-matrix interactions in basalt-fibre-reinforced geopolymer-matrix composites after heating, *J. Ceram. Sci. Tech,* **6**, [1], 17 – 24, (2015).

17 Thomas, S., Paul, S.A., Pothan, L.A., Deepa, B.: Natural fibres: structure, properties and applications, In: Cellulose Fibers: Bio-and Nano-Polymer Composites. 3 – 42. Springer Berlin Heidelberg, (2011).

18 Silva, F.A., Chawla, N., de Toledo Filho, R.D.: Tensile behavior of high performance natural (sisal) fibers, *Compos. Sci. Technol.*, **68**, 3438 – 3443, (2008).

19 Fidelis, M.E.A., Pereira, T.V.C., Gomes, O.D.F.M., de Andrade Silva, F., Toledo Filho, R.D.: The effect of fiber morphology on the tensile strength of natural fibers, *J. Mater. Res. Technol.,* **2**, 149 – 157, (2013).

20 Ramesh, M., Palanikumar, K., Reddy, K.H.: Mechanical property evaluation of sisal-jute-glass fiber reinforced polyester composites, *Compos. Part B: Eng.,* **48**, 1 – 9, (2013).

21 Wallis, A., Wearne, R., Wright, P.: Chemical analysis of polysaccharides in plantation eucalypt woods and pulps, *Appita J.,* **49**, [1], 258 – 262, (1996).

22 Borges, P.H., Banthia, N., Alcamand, H.A., Vasconcelos, W.L., Nunes, E.H.: Performance of blended metakaolin/blastfurnace slag alkali-activated mortars, *Cement Concrete Comp.*, **71**, 42 – 52, (2016).

23 ASTM C1437 – 15, Standard Test Method for Flow of Hydraulic Cement Mortar, ASTM International, West Conshohocken, PA, 2015.

24 ASTM C39/C39M-15a, Standard Test Method for Compressive Strength of Cylindrical Concrete Specimens, ASTM International, West Conshohocken, PA, 2015.

25 ASTM standard C1557, Standard Test Method for Tensile Strength and Young's Modulus of Fibers, ASTM International, West Conshohocken, PA, 2013.

26 Müller, C.M., Laurindo, J.B., Yamashita, F.: Effect of cellulose fibers on the crystallinity and mechanical properties of starch-based films at different relative humidity values, *Carbohyd. Polym.*, **77**, [2], 293 – 299, (2009).

27 Němeček, J., Šmilauer, V., Kopecký, L.: Nanoindentation characteristics of alkali-activated aluminosilicate materials, *Cement Concrete Comp.*, **33**, [2], 163 – 170, (2011).

28 Bernal S.A. *et al.*: Mechanical and thermal characterisation of geopolymers based on silicate-activated metakaolin/slag blends, *J. Mater. Sci.*, **46**, [16], 5477 – 5486, (2011).

[29] Bernal S.A. *et al.*: Performance of refractory aluminosilicate particle/fiber-reinforced geopolymer composites, *Compos. Part B: Eng.*, **43**, [4], 1919 – 1928, (2012).

[30] Van Riessen A. *et al.*: Thermo-mechanical and microstructural characterisation of sodium-poly (sialate-siloxo)(Na-PSS) geopolymers, *J. Mater. Sci.*, **42**, [9], 3117 – 3123, (2007).

[31] Ferreira, S.R., de Andrade Silva, F., Lima, P.R.L., Toledo Filho, R.D.: Effect of hornification on the structure, tensile behavior and fiber matrix bond of sisal, jute and curauá fiber cement based composite systems, *Constr. Build. Mater.*, **139**, 551 – 561, (2017).